XVI International Conference on Computational Plasticity. Fundamentals and Applications
COMPLAS 2021
E. Oñate, D. Peric, M. Chiumenti and Eduardo de Souza Neto (Eds)

ON SOLVING INCONSISTENCIES BETWEEN DIFFERENT TYPES OF HARDENING MODELS

STEVEN COOREMAN[*] ANDSAM COPPIETERS[†]

[*] ArcelorMittal Global R&D Gent / OCAS NV
Pres. J. F. Kennedylaan 3, 9060 Zelzate, Belgium
e-mail: steven.cooreman@arcelormittal.com, www.ocas.be

[†]KU Leuven, Department of Materials Engineering
Technology Campus Ghent
Gebroeders De Smetstraat 1, 9000 Gent, Belgium
email: sam.coppieters@kuleuven.be, https://iiw.kuleuven.be/onderzoek/mem2p

Key words: Advanced hardening models, Isotropic hardening, Kinematic hardening, Distortional hardening, Levkovitch-Svendsen model.

Abstract.*Over the past decades, many different phenomenological models have been developed; the simple ones only consider isotropic hardening and a von Mises yield surface, whereas the advanced models simultaneously account for the material's initial anisotropy and different types of hardening phenomena. The more advanced models are typically calibrated based on a rather extensive set of conventional mechanical tests such as tensile, tension-compression, tension-shear and tension-torsion tests. Furthermore, calibration is most often done in a sequential manner enabling to disentangle different phenomena.The Levkovitch-Svendsen model is such an advanced model accounting for isotropic, kinematic and distortional hardening and assuming Hill's 1948 yield criterion to capture the initial plastic anisotropy. The motivation for this paper was the observation that an unrealistically high anisotropic shear parameter was required to reproduce a torsion test when calibrating this model for an X70 steel grade. This observation is scrutinized in this paper through a numerical study.*

Tensile tests in the rolling and transverse direction and a torsion test around the transverse direction were simulated with different hardening models, thereby always assuming the same Hill 1948 yield criterion. First, these tests were simulated using a purely isotropic hardening model and assuming arbitrary strain hardening. These virtual experiments served as the ground-truth material response. It was then evaluated if those virtual experiments could be reproduced by means of an isotropic-kinematic and an isotropic-distortional hardening model. Even though monotonic stress paths were adopted in the virtual experiments, the isotropic-kinematic and the isotropic-distortional hardening model could not reproduce the virtual experiments generated by the purely isotropic hardening model. Thisseems to be an inconsistency complicating the calibration of more advanced constitutive models. However, in this paper it is shown that this inconsistency can be solved by scaling specific parameters in the evolution equations of the kinematic and distortional hardening model with a ratio of two equivalent stresses.

1 INTRODUCTION

Material forming and shaping through plastic deformation is still one of the most efficient and economic manufacturing processes and is therefore extensively used in many industries such as automotive, appliance, energy, etc. Since many years, FEA (Finite Element Analysis) is adopted to optimize metal forming processes, as it reduces the cost of the trial-and-error phase and the time-to-market.

An accurate description of the mechanical material behaviour is key for obtaining reliable FEA predictions. Over the past decades many phenomenological models have been developed; whereas the most simple ones assume that metals harden in an isotropic way, more advanced models are capable of capturing the metal's initial anisotropy [1, 2] and reproducing phenomena such as the Bauschinger effect and differential work hardening [3].

In general, one can distinguish between isotropic, kinematic and distortional hardening. Kinematic hardening refers to a translation of the yield surface in stress space and makes it possible to capture the Bauschinger effect. Well known kinematic hardening models are the linear models proposed by Prager [4] and Ziegler [5] and the non-linear model developed by Armstrong and Frederick [6]. Distortional hardening refers to a change of shape of the yield surface and allows reproducing phenomena such as cross-hardening, a phenomenon which manifests itself as an increase of the yield stress after orthogonal strain path changes [7, 8].

In 2007,Levkovitch and Svendsen proposed a phenomenological model which accounts for all three types of hardening and assumes Hill's 1948 yield criterion [1] to capture the material's initial anisotropy [9].A brief description of the model can be found in Section 2. The authors of this paper implemented this model in Abaqus by means of a UMAT user subroutine and adopted it to simulate spiral forming of large diameter welded pipes and to predict pipe properties from coil properties [10, 11]. To this end, the model was calibrated for an X70 steel grade, using data from tensile tests, cyclic tension-compression tests, torsion tests and tension-torsion tests. Furthermore, the different material parameters were calibrated in a sequential manner, enabling to disentangle different phenomena. However, it was observed that an unrealistically high anisotropic shear parameter was required to reproduce the torque–rotation angle curve from the torsion tests.

To investigate this observation, a numerical study was conducted, the results of which are presented in Sections 3 and 4 of this paper. The aim was to compare the mechanical behaviour predicted by an isotropic, a combined isotropic-kinematic and a combined isotropic-distortional hardening model in the case of monotonic stress paths, thereby always assuming the same Hill 1948 yield criterion. As will be shown in Section 3, it appears that the combined hardening models cannot reproduce the mechanical behaviour predicted by the isotropic hardening model, which seems to be an inconsistency complicating the calibration of more advanced constitutive models. Eventually, this inconsistency could be solved by scaling specific parameters in the evolution equations of the kinematic and distortional hardening model with a ratio of two equivalent stresses. Section 4 describes how these scaling factors were derived and presents the results from simulations with the modified hardening models.

2 LEVKOVITCH-SVENDSEN MODEL

The original Levkovitch-Svendsen model is presented in [9]. A slightly modified version was implemented by the authors. The yield function takes the following form:

$$\Phi = \sigma_{eq} - \sigma_y \leq 0 \tag{1}$$

The equivalent stressσ_{eq} is defined as:

$$\sigma_{eq} = \sqrt{(\boldsymbol{\sigma}^{dev} - \boldsymbol{\alpha}^{dev}) : (\boldsymbol{M} + \boldsymbol{H}) : (\boldsymbol{\sigma}^{dev} - \boldsymbol{\alpha}^{dev})} \tag{2}$$

$\boldsymbol{\sigma}^{dev}$ and $\boldsymbol{\alpha}^{dev}$ represent the deviatoric part of the Cauchy stress tensor $\boldsymbol{\sigma}$ and the backstress tensor $\boldsymbol{\alpha}$, respectively. $\boldsymbol{M}$ is a fourth order tensor of constants which describes the initial anisotropy of the material, while $\boldsymbol{H}$is a fourth order tensor which evolves with plastic deformation and thus describes the distortion of the yield surface. When assuming Hill's 1948 yield criterion and when using Voigt notation, the tensor $\boldsymbol{M}$ is defined as:

$$\boldsymbol{M} = \begin{bmatrix} G+H & -H & -G & 0 & 0 & 0 \\ -H & H+F & -F & 0 & 0 & 0 \\ -G & -F & G+F & 0 & 0 & 0 \\ 0 & 0 & 0 & 2N & 0 & 0 \\ 0 & 0 & 0 & 0 & 2M & 0 \\ 0 & 0 & 0 & 0 & 0 & 2L \end{bmatrix} \tag{3}$$

with$F$, G, H, M, N and L the parameters of Hill's 1948 yield criterion.

σ_y represents the size of the yield surface, which is a function of the equivalent plastic strain ε_{eq}^{pl}.

An associativeflow rule isapplied:

$$\boldsymbol{D}^{pl} = \dot{\lambda} \cdot \frac{\partial \Phi}{\partial \boldsymbol{\sigma}^{dev}} \tag{4}$$

With$\boldsymbol{D}^{pl}$ the plastic strain rate tensor and $\dot{\lambda}$ the plastic multiplier.

Theequivalentplasticstrainrateiscomputedbasedontheconventionthattheplasticwork per unit time and per unitvolumeshouldequaltheproductofthework-equivalent stress and theequivalentplasticstrainrate, or:

$$\dot{\varepsilon}_{eq}^{pl} = \frac{\boldsymbol{\sigma} : \boldsymbol{D}^{pl}}{\sigma_{eq}^{Work}} \tag{5}$$

withσ_{eq}^{Work} the work-equivalent stress, which is defined as:

$$\sigma_{eq}^{Work} = \sqrt{\boldsymbol{\sigma}^{dev} : \boldsymbol{M} : \boldsymbol{\sigma}^{dev}} \tag{6}$$

As proposedbyLemaître and Chaboche [12], the total backstress$\boldsymbol{\alpha}$ is defined as a summation of different backstresses $\boldsymbol{\alpha}_k$, where the evolution of each backstress is defined by the Armstrong-Frederick model [6]:

$$\dot{\boldsymbol{\alpha}} = \sum_{k=1}^{N} \dot{\boldsymbol{\alpha}}_k \tag{7}$$

$$\dot{\boldsymbol{\alpha}}_k = C_k \cdot \left(X_{sat,k} \cdot \boldsymbol{D}^{pl} - \boldsymbol{\alpha}_k \cdot \dot{\varepsilon}_{eq}^{pl} \right)$$

with$X_{sat,k}$ and C_k material parameters whichneedto be calibrated.

Theevolutionofthedistortionalhardening tensor $\boldsymbol{H}$ is described by the following equation:

$$\dot{\boldsymbol{H}} = \dot{\varepsilon}_{eq}^{pl} \cdot C_D \cdot (D_{sat} - H_D) \cdot \boldsymbol{N} \otimes \boldsymbol{N} + \dot{\varepsilon}_{eq}^{pl} \cdot C_L \cdot [L_{sat} \cdot (\boldsymbol{I}^{dev} - \boldsymbol{N} \otimes \boldsymbol{N}) - \boldsymbol{H}_L] \tag{8}$$

with:

- C_D, D_{sat}, C_L and L_{sat}, material parameters which havetobe calibrated
- $\boldsymbol{N}$, a second order tensor with Eucledian norm 1, parallel to $\boldsymbol{D}^{pl}$
- $\boldsymbol{N}\otimes\boldsymbol{N}$, a fourth order tensor
- H_D, the projection of $\boldsymbol{H}$ on $\boldsymbol{N}\otimes\boldsymbol{N}$, i.e. $H_D = H_{ijkl} \cdot N_{ij} \cdot N_{kl}$
- $\boldsymbol{H}_L = \boldsymbol{H} - H_D \cdot \boldsymbol{N}\otimes\boldsymbol{N}$
- $\boldsymbol{I}^{dev}$, the deviatoric fourth order unit tensor, whichisdefined as:

$$I_{ijkl}^{dev} = -\frac{1}{3}\cdot\delta_{ij}\cdot\delta_{kl} + \frac{1}{2}\cdot\delta_{ik}\cdot\delta_{jl} + \frac{1}{2}\cdot\delta_{il}\cdot\delta_{jk} \tag{9}$$

Theterm " $\dot{\varepsilon}_{eq}^{pl} \cdot C_D \cdot (D_{sat} - H_D) \cdot \boldsymbol{N}\otimes\boldsymbol{N}$" is referred to as directional hardening, as it results in hardening along the plastic strain rate direction$\boldsymbol{N}$, while the term " $\dot{\varepsilon}_{eq}^{pl} \cdot C_L \cdot [L_{sat} \cdot (\boldsymbol{I}^{dev} - \boldsymbol{N}\otimes\boldsymbol{N}) - \boldsymbol{H}_L]$ " is called the latent hardening part, because it generates hardening on the directions orthogonal to $\boldsymbol{N}$.

3 PROBLEM STATEMENT

To investigate the inconsistency described in the introduction, a numerical study was conducted in which tensile tests in RD (rolling direction) and TD (transverse direction) and a torsion test around TD were simulated with different hardening models. In all simulations, the initial plastic anisotropy was described by the Hill 1948 yield criterion, using the anisotropy parameters shown in **¡Error! No se encuentra el origen de la referencia.**.

First, the mechanical tests were simulated using a purely isotropic hardening model assuming arbitrary strain hardening. The stress-strain and torque-rotation angle curves obtained from those simulations were considered to be the ground-truth material response in the remainder of the study, referred to as the reference curves. Next, the same mechanical tests were simulated using a combined isotropic-kinematic hardening model and a combined isotropic-distortional hardening model. Kinematic and distortional hardening were described by the evolution equations presented in Section 2. Given that monotonic mechanical tests are considered in this study, only the directional hardening part plays a role of importance in the case of distortional hardening. Arbitrarily chosen values were assigned to the kinematic and directional hardening parameters. The isotropic hardening part of the combined hardening models was calibrated based on the reference stress-strain curve from the tensile test in RD. In theory, the combined hardening models should be able to reproduce the monotonic ground-truth mechanical tests, irrespective of the chosen kinematic and directional hardening parameters.

All results from those simulations are summarized in Figure 1. As can be observed, the combined hardening models predict the exact same behaviour as the purely isotropic hardening model for the tensile test in RD. However, they predict significantly different behaviour for the tensile test in TD and the torsion test. Thus, there seems to be an unexpected incompatibility between the hardening models considered in this study.

Table 1:parametersof Hill 1948 yieldcriterion

F	G	H	M	N	L
0.4	0.45	055	1.8	1.9	1.95

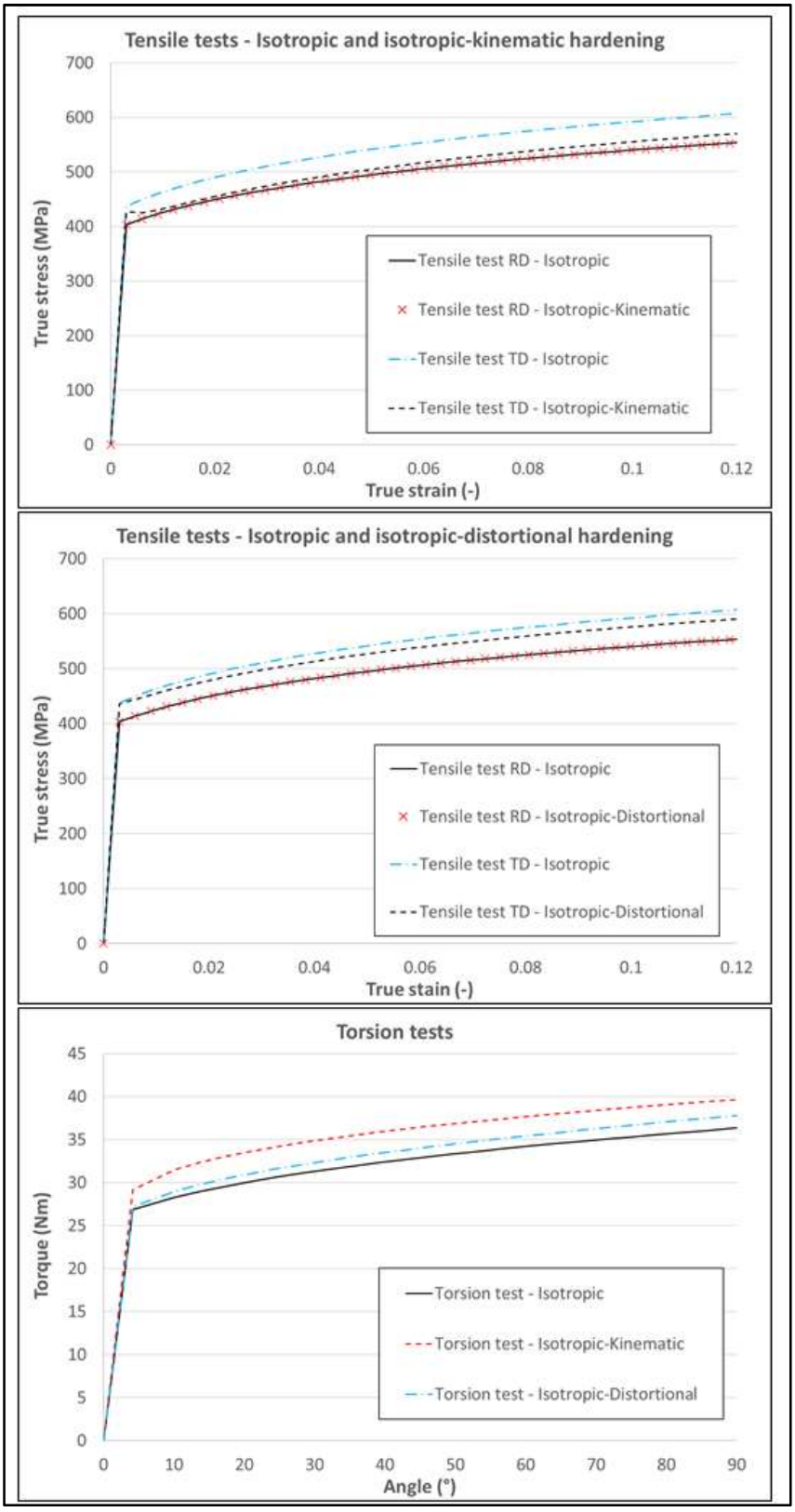

Figure 1: Results from simulations with original evolution equations

4 HOW TO SOLVE THE INCONSISTENCY

The inconsistency illustrated in Section 3 can be solved by scaling the saturation parameters X_{sat} and D_{sat}in the evolution equation of the backstress tensor $\boldsymbol{\alpha}$ (Equation (7)) and the distortional hardening tensor $\boldsymbol{H}$(Equation (8)), respectively. The key point is that those scaling factors should depend on the direction along which the material is deformed and were determined by the following reasoning. Assume two pure shear tests on the same material, one in the RD-TD plane and another in the RD-ND (normal direction) plane. In the formulas below, the directions RD, TD and ND are referred to as 1, 2 and 3, respectively. Furthermore, assume that the material's anisotropy is described by means of Hill's 1948 yield criterion and suppose that Hill parameter N, i.e. the anisotropy parameter related to shear stress σ_{12}, equals $3/2$, i.e. the von Mises value. Based on the principle of equivalent plastic work (Equation (5)), the following relations can be derived:

$$\sigma_{eq}^{Work} \cdot \dot{\varepsilon}_{eq}^{pl} = 2 \cdot \sigma_{12} \cdot \dot{\varepsilon}_{12}^{pl} = 2 \cdot \sigma_{13} \cdot \dot{\varepsilon}_{13}^{pl} \tag{10}$$

$$\dot{\varepsilon}_{eq}^{pl} = 2 \cdot \frac{\sigma_{12}}{\sigma_{eq}^{Work}} \cdot \dot{\varepsilon}_{12}^{pl} = 2 \cdot \frac{\sigma_{12}}{\sqrt{3} \cdot \sigma_{12}} \cdot \dot{\varepsilon}_{12}^{pl} = \frac{2}{\sqrt{3}} \cdot \dot{\varepsilon}_{12}^{pl}$$

$$\dot{\varepsilon}_{eq}^{pl} = 2 \cdot \frac{\sigma_{13}}{\sigma_{eq}^{Work}} \cdot \dot{\varepsilon}_{13}^{pl} = 2 \cdot \frac{\sigma_{13}}{\sqrt{2 \cdot M} \cdot \sigma_{13}} \cdot \dot{\varepsilon}_{13}^{pl} = \frac{2}{\sqrt{2 \cdot M}} \cdot \dot{\varepsilon}_{13}^{pl}$$

With M the anisotropy parameter related to shear stress σ_{13}.

In the case of purely kinematic hardening and assuming that the backstress evolves as described by Equation (7), the shear stresses σ_{12} and σ_{13} can be computed as specified in Equations (11) and (12):

$$\dot{\alpha}_{12} = C \cdot \left(X_{sat,12} \cdot \dot{\varepsilon}_{12}^{pl} - \alpha_{12} \cdot \dot{\varepsilon}_{eq}^{pl}\right) = C \cdot \left(X_{sat,12} \cdot \frac{\sqrt{3}}{2} \cdot \dot{\varepsilon}_{eq}^{pl} - \alpha_{12} \cdot \dot{\varepsilon}_{eq}^{pl}\right) \tag{11}$$

$$\xrightarrow{\varepsilon_{eq}^{pl} = \int \dot{\varepsilon}_{eq}^{pl} \cdot dt} \alpha_{12} = X_{sat,12} \cdot \frac{\sqrt{3}}{2} \cdot \left(1 - e^{-C \cdot \varepsilon_{eq}^{pl}}\right)$$

$$\dot{\alpha}_{13} = C \cdot \left(X_{sat,13} \cdot \dot{\varepsilon}_{13}^{pl} - \alpha_{13} \cdot \dot{\varepsilon}_{eq}^{pl}\right) = C \cdot \left(X_{sat,13} \cdot \frac{\sqrt{2 \cdot M}}{2} \cdot \dot{\varepsilon}_{eq}^{pl} - \alpha_{13} \cdot \dot{\varepsilon}_{eq}^{pl}\right)$$

$$\xrightarrow{\varepsilon_{eq}^{pl} = \int \dot{\varepsilon}_{eq}^{pl} \cdot dt} \alpha_{13} = X_{sat,13} \cdot \frac{\sqrt{2 \cdot M}}{2} \cdot \left(1 - e^{-C \cdot \varepsilon_{eq}^{pl}}\right)$$

Please note that, in the model, it is assumed that $X_{sat,12}$ equals $X_{sat,13}$, but here we differentiate between both to derive the scaling factor. Because we assume purely kinematic hardening, the size of the yield surface, defined as σ_y (Equation (1)), does not evolve. Thus:

$$\sigma_{eq} = \sigma_y = \sqrt{3} \cdot (\sigma_{12} - \alpha_{12}) = \sqrt{2 \cdot M} \cdot (\sigma_{13} - \alpha_{13}) \tag{12}$$

And, consequently, the shear stresses σ_{12} and σ_{13} read as:

$$\sigma_{12} = \frac{\sigma_y}{\sqrt{3}} + X_{sat,12} \cdot \frac{\sqrt{3}}{2} \cdot \left(1 - e^{-C \cdot \varepsilon_{eq}^{pl}}\right) \tag{13}$$

$$\sigma_{13} = \frac{\sigma_y}{\sqrt{2 \cdot M}} + X_{sat,13} \cdot \frac{\sqrt{2 \cdot M}}{2} \cdot \left(1 - e^{-C \cdot \varepsilon_{eq}^{pl}}\right)$$

By combining Equations (10) and (13), a relation between $X_{sat,12}$ and $X_{sat,13}$ can be derived:

$$2 \cdot \sigma_{12} \cdot \dot{\varepsilon}_{12}^{pl} = 2 \cdot \sigma_{13} \cdot \dot{\varepsilon}_{13}^{pl} \tag{14}$$

$$\rightarrow \sigma_{12} \cdot \frac{\sqrt{3}}{2} \cdot \dot{\varepsilon}_{eq}^{pl} = \sigma_{13} \cdot \frac{\sqrt{2 \cdot M}}{2} \cdot \dot{\varepsilon}_{eq}^{pl}$$

$$\rightarrow \frac{\sigma_{12}}{\sigma_{13}} = \frac{\frac{\sqrt{2 \cdot M}}{2}}{\frac{\sqrt{3}}{2}}$$

$$\rightarrow \frac{\frac{\sigma_y}{\sqrt{3}} + X_{sat,12} \cdot \frac{\sqrt{3}}{2} \cdot \left(1 - e^{-C \cdot \varepsilon_{eq}^{pl}}\right)}{\frac{\sigma_y}{\sqrt{2 \cdot M}} + X_{sat,13} \cdot \frac{\sqrt{2 \cdot M}}{2} \cdot \left(1 - e^{-C \cdot \varepsilon_{eq}^{pl}}\right)} = \frac{\frac{\sqrt{2 \cdot M}}{2}}{\frac{\sqrt{3}}{2}}$$

$$\rightarrow X_{sat,13} = X_{sat,12} \left(\frac{\sqrt{3}}{\sqrt{2 \cdot M}}\right)^2$$

The ratio $\left(\frac{\sqrt{3}}{\sqrt{2 \cdot M}}\right)^2$ can be written in a general way as the ratio of two equivalent stresses, namely $\left(\frac{\sigma_{eq}^{Mises}}{\sigma_{eq}^{Work}}\right)^2$, with σ_{eq}^{Mises} the work-equivalent Mises stress:

$$\sigma_{eq}^{Mises} = \sqrt{\boldsymbol{\sigma}^{dev} : \boldsymbol{M}^{Mises} : \boldsymbol{\sigma}^{dev}} \tag{15}$$

In Voigt notation, the fourth order tensor $\boldsymbol{M}^{Mises}$ can be written as:

$$\boldsymbol{M} = \begin{bmatrix} 1 & -1/2 & -1/2 & 0 & 0 & 0 \\ -1/2 & 1 & -1/2 & 0 & 0 & 0 \\ -1/2 & -1/2 & 1 & 0 & 0 & 0 \\ 0 & 0 & 0 & 3 & 0 & 0 \\ 0 & 0 & 0 & 0 & 3 & 0 \\ 0 & 0 & 0 & 0 & 0 & 3 \end{bmatrix} \tag{16}$$

The inconsistency between the isotropic and the combined isotropic-kinematic hardening model can be solved by multiplying the saturation parameters X_{sat} with the ratio $\left(\frac{\sigma_{eq}^{Mises}}{\sigma_{eq}^{Work}}\right)^2$, as will be illustrated further in the paper. The evolution equation of the backstress tensor then becomes:

$$\dot{\boldsymbol{\alpha}}_k = C_k \cdot \left(\left(\frac{\sigma_{eq}^{Mises}}{\sigma_{eq}^{Work}}\right)^2 \cdot X_{sat,k} \cdot \boldsymbol{D}^{pl} - \boldsymbol{\alpha}_k \cdot \dot{\varepsilon}_{eq}^{pl}\right) \tag{17}$$

In the same way, the scaling factor for the saturation parameter D_{sat} can be derived. In the case of purely distortional hardening (or purely directional hardening to be more precise) and assuming that distortional hardening is defined by Equations (1) and (8), the shear stresses $\sigma_{12}$and σ_{13} can be computed as specified in Equations (18) and (19):

$$\dot{H}_{1212} = \dot{H}_{1221} = \dot{H}_{2121} = \dot{H}_{2112} = C_D \cdot \left(D_{sat,12} - H_{1212}\right) \cdot \dot{\varepsilon}_{eq}^{pl} \tag{18}$$

$$\xrightarrow{\varepsilon_{eq}^{pl} = \int \dot{\varepsilon}_{eq}^{pl} \cdot dt} H_{1212} = H_{1221} = H_{2121} = H_{2112} = D_{sat,12} \cdot \left(1 - e^{-C_D \cdot \varepsilon_{eq}^{pl}}\right)$$

$$\dot{H}_{1313} = \dot{H}_{1331} = \dot{H}_{3131} = \dot{H}_{3113} = C_D \cdot \left(D_{sat,13} - H_{1313}\right) \cdot \dot{\varepsilon}_{eq}^{pl}$$

$$\xrightarrow{\varepsilon_{eq}^{pl} = \int \dot{\varepsilon}_{eq}^{pl} \cdot dt} H_{1313} = H_{1331} = H_{3131} = H_{3113} = D_{sat,13} \cdot \left(1 - e^{-C_D \cdot \varepsilon_{eq}^{pl}}\right)$$

The parameter σ_y does not evolve. Hence:

$$\sigma_{eq} = \sigma_y = \sqrt{4 \cdot H_{1212} + 3} \cdot \sigma_{12} = \sqrt{4 \cdot H_{1313} + 2 \cdot M} \cdot \sigma_{13} \tag{19}$$

$$\rightarrow \sigma_{12} = \frac{\sigma_y}{\sqrt{4 \cdot D_{sat,12} \cdot \left(1 - e^{-C_D \cdot \varepsilon_{eq}^{pl}}\right) + 3}}$$

$$\rightarrow \sigma_{13} = \frac{\sigma_y}{\sqrt{4 \cdot D_{sat,13} \cdot \left(1 - e^{-C_D \cdot \varepsilon_{eq}^{pl}}\right) + 2 \cdot M}}$$

By combining Equations (10) and (18), a relation between $D_{sat,12}$ and $D_{sat,13}$ can be derived:

$$\frac{\sigma_{12}}{\sigma_{13}} = \frac{\frac{\sqrt{2 \cdot M}}{2}}{\frac{\sqrt{3}}{2}} \tag{20}$$

$$\rightarrow \frac{\frac{\sigma_y}{\sqrt{4 \cdot D_{sat,12} \cdot \left(1 - e^{-C_D \cdot \varepsilon_{eq}^{pl}}\right) + 3}}}{\frac{\sigma_y}{\sqrt{4 \cdot D_{sat,13} \cdot \left(1 - e^{-C_D \cdot \varepsilon_{eq}^{pl}}\right) + 2 \cdot M}}} = \frac{\frac{\sqrt{2 \cdot M}}{2}}{\frac{\sqrt{3}}{2}}$$

$$\rightarrow D_{sat,13} = D_{sat,12} \left(\frac{\sqrt{2 \cdot M}}{\sqrt{3}}\right)^2$$

The ratio $\left(\frac{\sqrt{2 \cdot M}}{\sqrt{3}}\right)^2$ can also be written in a more general way as the ratio of two equivalent stresses, namely $\left(\frac{\sigma_{eq}^{Work}}{\sigma_{eq}^{Mises}}\right)^2$. The inconsistency between the isotropic and the combined isotropic-distortional hardening model can thus be solved by multiplying the saturation parameter D_{sat} with the ratio $\left(\frac{\sigma_{eq}^{Work}}{\sigma_{eq}^{Mises}}\right)^2$. The evolution equation of the fourth order distortional hardening tensor then becomes:

$$\dot{\boldsymbol{H}} = \dot{\varepsilon}_{eq}^{pl} \cdot C_D \cdot \left(\left(\frac{\sigma_{eq}^{Work}}{\sigma_{eq}^{Mises}}\right)^2 \cdot D_{sat} - H_D\right) \cdot \boldsymbol{N} \otimes \boldsymbol{N} + \dot{\varepsilon}_{eq}^{pl} \cdot C_L \cdot \left[L_{sat} \cdot \left(\boldsymbol{I}^{dev} - \boldsymbol{N} \otimes \boldsymbol{N}\right) - \boldsymbol{H}_L\right] \tag{21}$$

One can raise the question if the saturation parameter L_{sat} should also be scaled, but there is no reason to do so from a numerical point of view.

Finally, the tensile and torsion tests described in Section 3 were simulated with the

modified evolution equations for kinematic and distortional hardening. The results from those simulations are summarized inFigure 2. As can be observed, the different hardening laws predict exactly the same behaviour for the monotonic virtual mechanical tests considered in this study. Thus, scaling the saturation parameters X_{sat} and D_{sat} with a ratio of two equivalent stresses could solve the observed inconsistency. By scaling those saturation parameters, the amount of kinematic and directional hardening depends on the loading direction with respect to the principal material directions.

5 CONCLUSIONS

A numerical study was performed to compare the mechanical behaviour predicted by an isotropic, a combined isotropic-kinematic and a combined isotropic-distortional hardening model in the case of monotonic tests. It was expected that the different hardening models would be able to predict the same behaviour for monotonic stress paths, but this was not the case for the models considered in this study. This seems to be an inconsistency complicating the calibration of more advanced constitutive models. As shown and substantiated in this paper, this inconsistency can be solved by scaling the saturation parameters in the evolution equations of the kinematic and distortional hardening model with a ratio of two equivalent stresses.

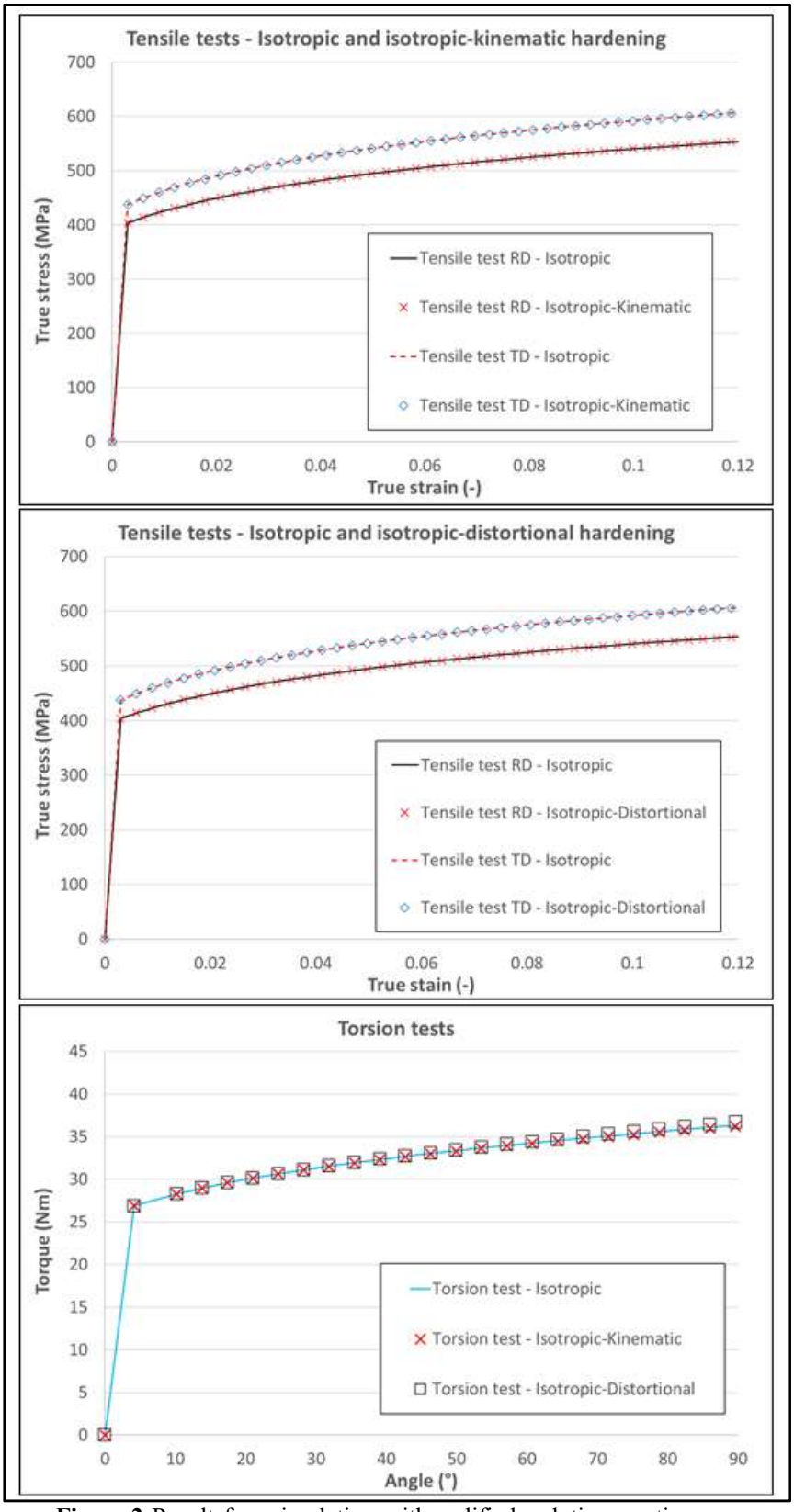

Figure 2: Results from simulations with modified evolution equations

REFERENCES

[1] Hill, R. A Theory of the yielding and plastic flow of anisotropic metals. *Proceedings of Royal Society of London*(1948), May 27.

[2] Barlat, F., Brem J. C., Yoon, J. W., Chung, K., Dick, R. E., Lege, D. J., Pourboghrat, F., Choi, S.-H. and Chu, E. Plane stress yield function for aluminum alloy sheets – part 1: theory.*Int. J. Plasticity* (2003) **19**:1297-1319.

[3] Ichikawa, K., Kuwabara, T. and Coppieters, S. Forming simulation considering the differential work hardening behavior of a cold rolled interstitial-free steel sheet. *Proceedings of the 17th Conference of the European Scientific Association of Metal Forming (ESAFORM)*(2014), May 7-9, Espoo, Finland.

[4] Prager, W. A new method of analyzing stresses and strains in work-hardening plasticsolids. *J. Appl. Mech.* (1956) **23**:493-496.

[5] Ziegler, H. A modification of Prager's hardening rule. *Appl. Math.* (1959)**17**:55-65.

[6] Armstrong, P. and Frederick, C. A mathematical representation of the multiaxial Bauschinger effect. *CEGB Repo*rt RD/B/N 731 (1966).

[7] Barthel, C., Levkovitch, V. and Svendsen, B. Modeling of sheet metal forming taking into account distortional hardening. *Int. J. Mater. Form.* (2008) **1**: 105-108.

[8] Barlat, F., Gracio, J. J., Lee, M.-G., Rauch, E. F. and Vincze, G. An alternative to kinematic hardening in classical plasticity. *Int. J. Plasticity* (2011) **27**:1309-1327.

[9] Levkovitch, V., Svendsen, B., Aydin, M. and Kessler, L. Accurate hardening modeling as basis for the realistic simulation of sheet forming processes with complex strain-path changes. *Proceedings of LS-Dyna Anwenderforum* (2007), Frankenthal, Germany.

[10] Cooreman, S., Van Hoecke, D., Liebeherr, M., Thibaux, P. and Luccioni, H. Advanced constitutive model for the accurate evaluation of the structural performance of welded pipes in offshore applications. *Proceedings of the 12th International Pipeline Conference* (2018), September 28 – October 2, Calgary, Alberta, Canada.

[11] Cooreman, S., Van Hoecke, D., Abotula, S., Luccioni, H., Voudouris, N. and Tazedakis, A. Prediction of properties on large diameter welded pipe: case study on 32" x 16mm X65 HSAW pipe. *Proceedings of Technology for Future and Aging Pipelines Conference* (2021), October 19-21, Gent, Belgium.

[12] Chaboche, J. L., Dang Van, K. and Cordier, G. Modelization of the strain memory effect on the cyclic hardening of 316 stainless steel. *Proceedings of the 5th International Conference on Structural Mechanics in Reactor Technology* (1979), Division L11/3, Berlin, Germany, August 13-17.